

NUMERICAL SIMULATION OF A GROUND-BASED ADAPTIVE TELESCOPE

V.P. Lukin, N.N. Maier, and B.V. Fortes

*Institute of Atmospheric Optics,
Siberian Branch of the Academy of Sciences of the USSR, Tomsk*

Received September 26, 1991

We analyze the effectiveness of phase correction of distortions introduced in the wave by fluctuations of the refractive index of the atmosphere in the formation of images of astronomic objects. Two methods of modelling the phase distortions are described, based on generation either an ensemble of spectral amplitudes or random coefficients of aberrations. These methods are simultaneously used in the calculations.

Atmospheric turbulence is known to limit the angular resolution up to about 1 second of arc for observations of astronomical objects while the diffraction resolution is about 0.03 second of arc for observations made in the optical range ($\lambda \approx 0.5 \mu\text{m}$) with a telescope 3.6 m in diameter. There are three principal approaches to the problem of improving the resolution of an astronomical instrument:

1. Recording of an ensemble of short-exposed images and their subsequent processing with the use of the correlation methods (speckle-interferometry);¹
2. Measurements of phase distortions of the wavefront and correction of these distortions in the course of observations (adaptive methods);²
3. Simultaneous recording of short-exposed images and phase distortions of the wavefront of a reference source (beacon) with their subsequent processing.

We will consider a telescope equipped with a system of correction of phase distortions of the wavefront. Lately considerable attention is devoted to the equipment of the available telescopes with such systems.^{6,7} At present at least three possible fields of astronomical investigations can be found in which the adaptive methods are widely used: 1) spectrographic observations based on recording of the spectrum of the investigated object which simultaneously is a reference source for the system of recording of phase distortions of the wavefront, 2) studies of a protoplanet medium around the bright stars, in this case adaptive compensation reduces scattering on the coronagraph optics, and 3) resolving the double and multiple stars with further processing of their short-exposed images by speckle-interferometric methods or even without processing. In each of these cases adaptive methods reduce the time needed to record the astronomical information thereby improving the telescope performance. Thus constructing the adaptive telescope would be equivalent to designing a number of instruments without adaptive compensation.

In this paper we present the results of calculation of the point spread function of the adaptive telescope with a circular aperture 1 m in diameter for the monochromatic wavelength $\lambda = 0.55 \mu\text{m}$. We are going to include a program imitating the operation of the wavefront sensor in our numerical model, but so far assume the phase distortions in the incident wave to be well known, and the results of our calculations illustrate only the limitations due to the finite number of the degrees of freedom of the phase corrector. We consider two types of phase correctors: the modal corrector, which compensates for aberrations from tilt to coma and the segmented mirror with a hexagonal structure. In contrast to Refs. 9 and 10, our program permits us to vary the number of elements in the segmented mirror. In addition, the authors of Refs. 5, 9, and 10 have

not considered the effectiveness of aberration correction with a modal corrector.

MODELING THE TURBULENT DISTORTIONS OF THE PHASE

The technique employed for modeling the phase distortions introduced in a plane monochromatic wave by turbulent inhomogeneities of the atmospheric refractive index differs from the well-known techniques described in Refs. 5, 8, and 9, although it is also based on the Fourier transform of the spectral amplitude of the phase distortions. Essentially our scheme incorporates two independent programs. One of them generates the phase distortions by the method of the Fourier transform. The spatial scale of these distortions is limited from below by the step size and from above – by the computational grid size. The second program recalculates the scales larger than the computational grid size into classic aberrations, which are assumed to be random Gaussian variables with zero mean and variance being equal to¹¹

$$\sigma_n^2 = 8\pi(n+1) \int \Phi(k) \frac{J_{n+1}^2(\kappa R)}{(\kappa R)^2} \kappa d\kappa,$$

where n is the radial power of the corresponding polynomial, R is the radius of the circle, J is the Bessel function, $\Phi(\kappa) = 0.489 r_0^{-5/3} \kappa^{-11/3}$ is the spatial spectrum of phase distortions, and r_0 is Fried's radius of coherence. The upper limit of integration over κ is taken to be $2\pi/G$, where G is the size of the computational grid.

Random aberrations prescribed in such a way were added to phase distortions generated within the computational grid by the method of the Fourier transform. The essence of this method consists in calculation of the discrete Fourier transform of a random realization of the discrete analogue of spectral amplitude $F(\kappa_x, \kappa_y)$ obeying the relation $\langle |F(\kappa_x, \kappa_y)|^2 \rangle = \Phi(\kappa_x, \kappa_y)$. This condition does not yield an unambiguous definition of the statistics of the complex field F , and for this reason a certain uncertainty retains in the possible way of generating the ensemble F . We solve this problem in the following way: we assume the value $|F|$ to be deterministic, so that $|F| = \Phi^{1/2}$ and $\arg F$ is a random value uniformly distributed on the interval $[-\pi, \pi]$. In addition, we impose a condition $F(-\kappa_x, \kappa_y) = F^*(\kappa_x, \kappa_y)$ which ensures the two-dimensional discrete Fourier transform of the field F to be real. This technique was tested in the following way: the constant and

the linear components (tilt) were eliminated from the circle of the diameter D , then the variance of the phase was calculated within this circle. The variance was averaged over the ensemble of realizations and compared with its theoretical value $\Delta_3 = 0.134 (D/r_0)^{5/3}$ (see Ref. 11). This test demonstrated a good agreement between analytic and the calculated values of Δ_3 .

Thus our method of modeling the turbulent distortions has the following advantages over the well-known methods: first, the radius of atmospheric coherence r_0 is an input but not estimated parameter of the problem, in contrast, for example, to Ref. 10; second, the method makes it possible to account for the scales larger than the size of computational grid; and third, the random spectral amplitude of distortions is generated in such a way that the phase distortions appear to be real (otherwise, the energy of their spectrum is divided between real and imaginary parts of the output array).

In our paper we present the results obtained by means of a statistical averaging of the image. Further we plan to model the dynamic process of phase correlation. Now a program has been constructed which generates random realizations of the aberration coefficients $a_l(t)$ as functions of time. This program can be used not only for modeling the dynamics of the phase distortions generated by the motion of turbulent inhomogeneities whose size is larger than the size of the computational grid but also for studying the dynamic characteristics of the atmospheric phase distortions and of the residual phase distortions in the adaptive system. The following parameters were prescribed as input: inner and outer scales of turbulence,

the Fried radius of coherence, the angle \hat{v} between the wind direction and the OX axis, the wind velocity v , and the radial power n and the azimuthal frequency m of Zernike polynomials describing aberrations we are interested in. In the first part of the program we calculated the correlation function of the corresponding aberration coefficient.³

$$B(\tau) = 8\pi(n+1) \times \int \Phi(k) \frac{J_{n+1}^2(\kappa R)}{(\kappa R)^2} [J_0(\kappa v \tau) \pm \delta_{om} (-1)^m \times \\ \times J_{2m}(\kappa v \tau) \cos(2m \hat{v})] \kappa d\kappa.$$

The sign plus here corresponds to the cosine polynomial, the sign minus $-$ to the sine polynomial, and δ is Kronecker's delta symbol. In second part of the program we calculated the spectrum of the aberration coefficient

$$W(f) = 2 \int_0^\infty d\tau B(\tau) \cos 2\pi f \tau.$$

The spectrum $W(f)$ may be calculated in two different ways: either by calculating the integral over κ after it has been analytically calculated over τ , or by the cosine

transform of the discrete representation of the correlation function $B(\tau)$. The random realization $a_l(t)$ was generated by the method analogous to that which was used to obtain the random realizations of the phase distortions.

RESULTS OF CALCULATION OF THE POINT SPREAD FUNCTION (PSF)

We now proceed to the discussion of the calculated results. Averaging the random realizations of the PSF over the ensemble, we obtained the long-exposed distribution of the intensity $I(\gamma_x, \gamma_y)$ in the image plane. Then the fraction of energy within the circle of the radius ω (the value of ω in Figs. 1, 2, and 3 is given in seconds of arc)

$$E(\omega) = \frac{\int \int_{\gamma_x^2 + \gamma_y^2 < \omega^2} I(\gamma_x, \gamma_y) d\gamma_x d\gamma_y}{\int \int I(\gamma_x, \gamma_y) d\gamma_x d\gamma_y}.$$

was calculated. Recall that calculations were made for the telescope of the diameter D equal to 1 m with the radius of coherence r_0 being equal to 10 and 20 cm. Each figure shows the dependences corresponding to the diffraction (dashed curve) and uncorrected (dot-dash curve) cases. The following calculations were run for the modal corrector: 1) correction of total tilt; 2) correction of total tilt, defocusing, and astigmatism; and, 3) correction of total tilt, defocusing, astigmatism, and coma. The calculations were performed for the segmented corrector with 7, 19, and 37 elements, and total tilt was preliminarily eliminated from the aperture of the input pupil. Each segment had one, two or three degrees of freedom corresponding to compensation for either the constant component or the local tilts or both of them within each individual segment. We do not show the graphs corresponding to the regime of compensation for local tilts in the figures, because such a compensation did not result in any noticeable increase in $E(\alpha)$ in comparison with the regime of compensation for total tilt over the entire aperture. It can be seen from the figures that the correction of the local average phase with the segmented mirror provides manifold increase in the fraction of energy within the circle of the diffraction size $\lambda/D \approx 0.1''$ while in the case in which the local average phase and tilts were corrected with the segmented mirror the energy distribution $E(\omega)$ approached the diffraction one with the number of segments either 19 or 37. The correction of aberrations from tilt to coma, inclusively, also provides the satisfactory result for $r_0 = 20$ cm and $D/r_0 = 5$. However, the effectiveness of such a correction rapidly decreases when the optical strength of the atmospheric turbulence increases up to $r_0 = 10$ cm. The lowest curves in all figures correspond to the image formed without phase correction. It can be seen that the radius of the circle, in which 80% of energy is concentrated, is $0.55''$ for $r_0 = 20$ cm, and is $1.1''$ for $r_0 = 10$ cm. This agrees quite well with the well-known data of astronomical observations.

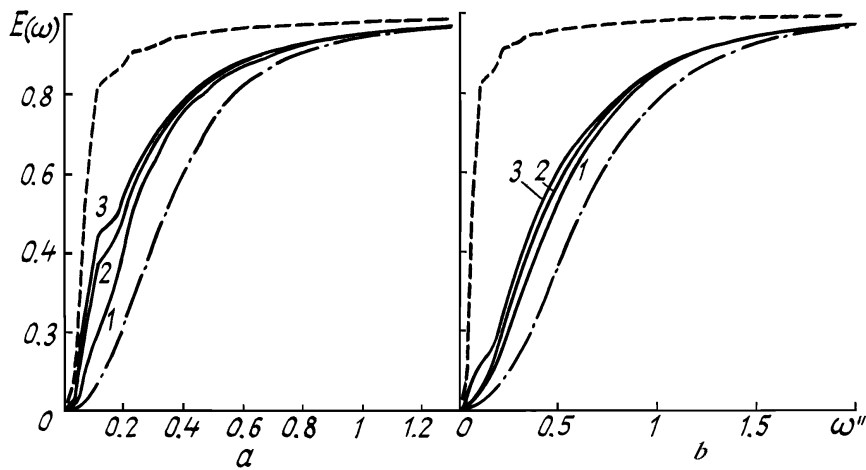


FIG. 1. Energy distribution of the distorted PSF after compensating for: 1) tilt; 2) tilt, defocusing, and astigmatism; and, 3) tilt, defocusing, astigmatism, and coma. Dashed curve shows the diffraction dependence and dot-dash curves correspond to the distortions introduced by the atmospheric turbulence: a) $r_0 = 20$ cm; b) $r_0 = 10$ cm.

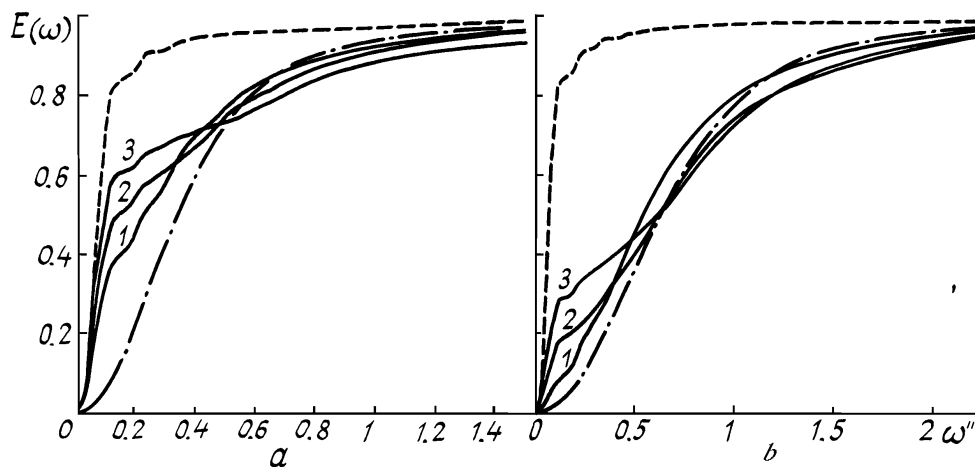


FIG. 2. Energy distribution of the distorted PSF after compensating for average phase with the segments of the 7-, 19-, and 37-element mirrors (curves 1, 2, and 3, respectively); dashed curve shows diffraction dependence and dot-dash curve corresponds to the distortions introduced by the atmospheric turbulence: a) $r_0 = 20$ cm and b) $r_0 = 10$ cm.

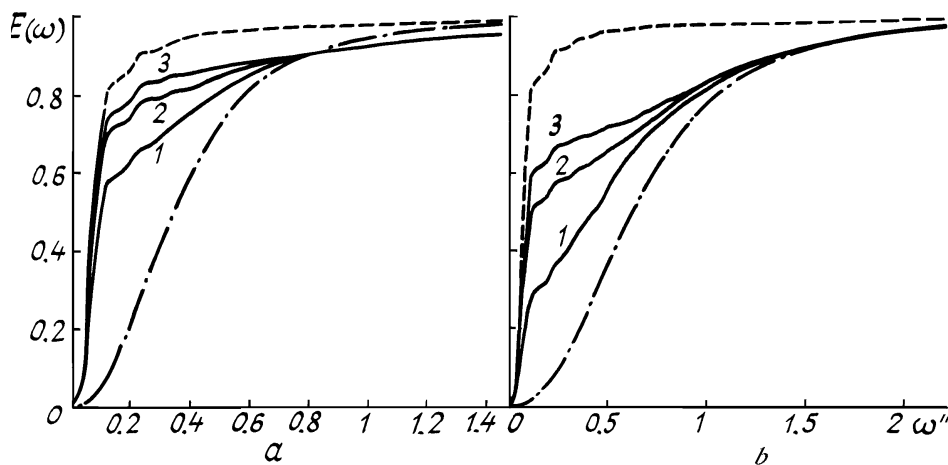


FIG. 3. Energy distribution of the distorted PSF after compensating for the average phase and local tilts with the segments of the 7-, 19-, and 37-element mirrors: a) $r_0 = 20$ cm and b) $r_0 = 10$ cm. Dashed curve shows the diffraction dependence and dot-dash curve corresponds to the distortions introduced by the atmospheric turbulence.

REFERENCES

1. J.W. Hardy, Proc. IEEE **66**, 651–680 (1978).
2. A. Labeyrie, Astron. Astrophys., No. 6, 85–87 (1970).
3. V.P. Lukin, *Atmospheric Adaptive Optics* (Nauka, Novosibirsk, 1986), 248 pp.
4. P.A. Konyaev, in: *Applied Mathematical Software* (Nauka, Novosibirsk, 1986), pp. 69–74.
5. P.A. Konyaev and N.N. Maier, Atm. Opt. **2**, No. 5, 474–478 (1989).
6. F. Merkle, Tech. Rept. LEST Foundat., No. 28, 117–130 (1987).
7. J.M. Beckers, F.J. Roddier, P.R. Eisenhardt, et al., SPIE **628**, 290–297 (1986).
8. J.M. Martin and S.M. Flatte, Apl. Opt. **27**, No. 11, 2111–2126 (1988).
9. R.C. Smithson and M.L. Peri, J. Opt. Soc. Am. **6**, No. 1, 92–97 (1989).
10. R.C. Smithson, M.L. Peri, and R.S. Benson, Apl. Opt. **27**, No. 8, 1615–1620 (1988).
11. R.J. Noll, J. Opt. Soc. Am. **66**, No. 3, 207–211 (1976).